

Single Image Super Resolution - When Model Adaptation Matters

Yudong Liang, Radu Timofte, *Member, IEEE*, Jinjun Wang, *Senior Member, IEEE*, Yihong Gong, *Senior Member, IEEE*, and Nanning Zheng, *Fellow, IEEE*

Abstract—In the recent years impressive advances were made for single image super-resolution. Deep learning is behind a big part of this success. Deep(er) architecture design and external priors modeling are the key ingredients. The internal contents of the low resolution input image is neglected with deep modeling despite the earlier works showing the power of using such internal priors. In this paper we propose a novel deep convolutional neural network carefully designed for robustness and efficiency at both learning and testing. Moreover, we propose a couple of model adaptation strategies to the internal contents of the low resolution input image and analyze their strong points and weaknesses. By trading runtime and using internal priors we achieve 0.1 up to 0.3dB PSNR improvements over best reported results on standard datasets. Our adaptation especially favors images with repetitive structures or under large resolutions. Moreover, it can be combined with other simple techniques, such as back-projection or enhanced prediction, for further improvements.

Index Terms—Internal prior, model adaptation, Deep convolutional neural network, Projection skip connection.

I. INTRODUCTION

SINGLE image super-resolution (SR) is a fundamental yet challenging vision problem of high practical and theoretical value. It is a particularly interesting problem as 4K images, videos and displays are of huge demands nowadays and most digitally recorded media used lower resolutions. Single image super-resolution aims at reconstructing a high resolution (HR) image for a given low resolution (LR) input. It is an ill-posed problem as usually to a low-resolution image patch there is a large number of corresponding high-resolution image patches. Numerous attempts have been made to solve this under-constrained or ill-posed problem. The techniques can be roughly divided into three categories: the interpolation methods [1], the reconstruction methods [2], [3], and the example based methods [4], [5], [6]. These methods exploit priors ranging from simple ‘smoothness’ priors applied in interpolation to more sophisticated statistical priors learned from large collections of natural images or from internal examples extracted from the low resolution image. Local structures, patterns, or textures tend to reappear many times across natural images [4], [5], [6], and even redundantly recur within the same image of the same scale or across different scales of the image [7], [8], [9]. The recurrence priors between LR and

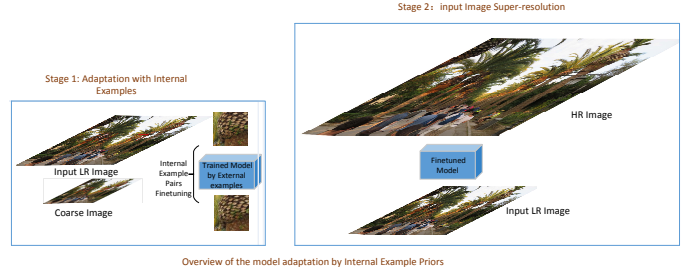


Fig. 1. Overview of our model adaptation strategy by internal example priors. The finetuned model has been trained using external examples.

HR image examples are modeled by learning a mapping from internal examples [4], [7], external examples [10], [6], [11] or from combined sources [12], [13].

The example based methods are the main research direction of the recent years. They refer to the priors from examples to restore missing details (high frequencies) in addition to the LR input information (low frequencies). These priors regulate the ill-posed super-resolution problem and help to obtain sharper and more visual pleasing results. In order to cover the high diversity of contents present in the natural images the external priors are usually extracted from large collections of LR/HR image example pairs. As demonstrated by many works [14], [13], [15], the amount of external train examples has a strong influence on the performance of the trained methods. On the other side, although the number of internal examples which come from the same input LR image or the scaled version is limited, the predictive power of the internal priors [7], [8], [9] is often stronger than that of the external priors. The internal priors are specific to the LR image and match the contextual and semantic information and the contents, while the external priors often embed generic and sometimes irrelevant information for a specific LR image. Patch redundancy or self-similarity probability of (small) image patches within the same scale or across a pyramid of scales of a natural image generally increases with the size of the image. With the development of the camera sensors the sizes of the photos continuously increase and indicate potential for exploiting internal priors as more internal examples can be used for an image specific adaptation SR process.

Internal priors are also widely applied in other image restoration applications, such as image denoising [16], [17]. Yang *et al.* [12] proposed a regression model for image superresolution by leveraging external examples and internal self-examples. The power of combination of internal priors and

Yudong Liang, Jinjun Wang, Yihong Gong and Nanning Zheng are with the Institute of Artificial Intelligence and Robotics, Xi'an Jiaotong University, China

Radu Timofte is with Computer Vision Laboratory, Department of Information Technology and Electrical Engineering, ETH Zürich, Switzerland.

external priors calls for a effective way to further improve the superresolution restoration.

Among example based methods, the learning based methods such as sparse coding [5], neighbor embedding [10], [6], [18] and recent deep learning based methods [15], [14] have largely promoted the performance of the SR process. Dong *et al.* [15], [11] proposed for SR the first successful deep convolutional neural network (CNN) termed SRCNN of three convolutional layers. SRCNN indicates the importance of feature representation which enjoy the merits of CNNs. However, SRCNN have failed to improve the performance by increasing the depth due to the difficulty of training. Inspired by the great success of deeper models in other computer vision tasks like image classification [19], [20], [21], Kim *et al.* [14] proposed a very deep CNN (VDSR) with depth up to 20 to predict the residual image. It applies a simple plain stacking network to predict the residual between the HR and LR images, which largely boosted the convergence speed and performance. It demonstrated again that the representational ability is very important to the single image SR problem.

Although VDSR has achieved impressive results, the plain structure of VDSR which simply stacks layers suffers gradient exploding/vanishing problem as network goes deeper. The convergence of deeper architectures becomes more difficult. The success of residual networks [21], [19] indicates the importance of skip connection in the information propagation. Another intuitive observation is that the simple stacking of too many ReLU layers has lost too much information. Dong *et al.* [22] has reported the use of PReLU has alleviated the ‘dead feature’ problem caused by zero gradients of ReLU layers. Alternatively, we propose a novel projection skip connection to preserve the negative information and to alleviate the gradient exploding/vanishing problem. With the idea to preserve negative information, a modification of reconstruction parts that discards ReLU layers has been proposed to cooperate with information propagation of projection skip connection. To avoid the overfitting and computational problem, we propose a Deep Projection convolution neural Network (DPN) with progressive pyramidal architecture which despite going deeper (40 layers vs. 20 layers) does not surpass the number of parameters from VDSR.

With DPN, our new design of deep architecture, we obtain state of the art performance with a learned model on external examples. The difficulty for training has been largely alleviated by our architecture. For a certain amount of data, the discriminative ability of the data to the problem is highly relevant to performance of the model. We hope to arouse the interests of communities for model adaptation with internal examples. To do model adaptation to a given image we propose a simple but effective method – finetuning of the external and offline learned model with internal examples as depicted in Fig. 1. The performance is further boosted with such an adaptation to each test image. Note that in all our experiments the adapted models perform comparable or better than the externally trained one. We validate the generality of our model adaptation strategy also when starting from VDSR.

In this paper, we make the following main contributions:

- 1) we present a novel deep model – DPN with performance,

robustness and easiness to train merits *w.r.t.* state-of-the-art VDSR model;

- 2) we propose and study a couple of model adaptation techniques as effective ways to significantly improve the performance of single image super-resolution methods;
- 3) we contribute an accurate model selection strategy based on observed image cross-scale content similarity and model performance correlation.

The remainder of the paper is structured as follows. Section II introduces our deep architecture and the proposed methods. Section III describes the experiments and the achieved results. Section V tries to share some insights and take-home messages. Section VI concludes the paper.

II. PROPOSED METHOD

First, we introduce the architecture of our Deep Projection convolutional neural Network (DPN) and discuss the motivations behind its design. Then, we propose a couple of model adaptation strategies to the internal contents of the LR input image, including a model selection strategy from adaptation, and analyze their strong points and weaknesses.

A. Motivation of the proposed deep architecture

Single image super-resolution also enjoys the performance benefits of deeper architectures. However, with plain stacking of convolutional layers and ReLU layers come also training difficulties [19]. Gradient exploding/vanishing problem is the main issue. Stacking the convolutional layer with ReLU layer outputs non-negative values which may impact the representational ability in SR. Moreover, overfitting may exist for certain low amount of train data. We tackle these problems by proposing our novel Deep Projection convolutional neural Network (DPN) depicted in Fig. 2. DPN has three parts: feature extraction/representation, inference, and reconstruction. The feature extraction part are plain stacking convolutional and ReLU layers as usual, the inference part consists of projection units and the reconstruction only applies convolutional layers to restore HR images. The projection design (see Fig.3a)) is meant to reduce the training difficulties and to preserve information as complete as possible at the same time, which makes the training more efficient and more robust.

Inspired by the deep residual CNN [19] and identity mapping deep CNN [21], gradient vanishing problem can be largely alleviated by skip connections or shortcuts. The calculation of residual unit can be as follows

$$x_{k+1} = x_k + F(x_k, W_k) \quad (1)$$

where x_k is the input of the unit and F is a function of x_k with parameters W_k .

The shortcuts decrease the difficulty of training but identity shortcuts are not sufficient to make up for the information loss due to non-negative outputs. Intuitively, the outputs need a refinement such

$$x_{k+1} = G(x_k) + F(x_k, W_k) \quad (2)$$

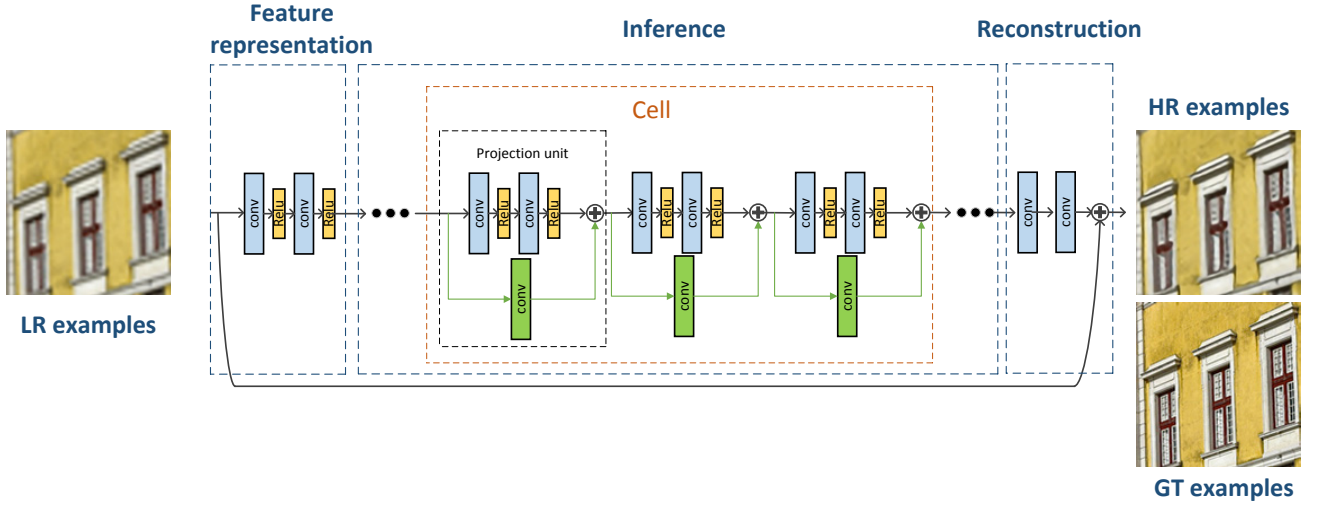


Fig. 2. The architecture of our deep projection convolutional neural network (DPN).

where G can be a function with an output in $[-\infty, \infty]$. The G behaves like a shortcut which is expected to be simple. A natural choice is a convolutional operation as in Fig. 3a). The non-negative output $F(x_k, W_k)$ brings non-linearity and projection $G(x_k)$ extends the descriptive ability. Thus, the inference part preserves information and alleviates the training difficulties. In combination with inference part, stacking convolutional layers only is applied in the reconstruction parts, otherwise with ReLU layers losing too much information at the end may impact the performance. Our designing philosophy coincides with [22] which uses PReLU for increasing the representation power. Our reconstruction part makes our net more stable, more robust and training more efficient as showed by the experiments.

The overfitting problem arises when the number of learned model parameters is too large for a given amount of train data. At the same time, for a good descriptive ability the network needs to be deep with a sufficient number of filters. In our DPN we increase the number of filters in a progressive pyramidal fashion and go deeper but without more parameters than VDSR.

The motivations to design the introduced CNN architectures include: 1) it adopts projection skip connections to allow for deeper structure; 2) the projection unit introduces extra convolution to increase the model capacity and preserves negative information; 3) integrating reconstruction part reduces the information loss; and 4) the design of the net complexity in a progressive pyramidal fashion controls the parameter numbers to be no more than VDSR. Experimentally, our implementation outperforms our reimplementation of VDSR for more than 0.1dB, which validates the strength of our proposed model structure.

B. Architecture

Our Deep Projection convolutional neural Network (DPN) is composed of several *Cells* which have certain number of projection units as shown in Fig. 2. Each unit consists of a summation between the output of 2 stacked conv+ReLU and

the output of a conv layer as in Fig. 3. All the convolutional layers have a receptive field of 3×3 . For succinctness in our implementation:

- The filter and channel numbers of the each projection unit in the cell i are the same, denoted as N_i .
- The numbers of the projection units in each cell are the same, k .
- Each cell is described as a collection of projection units, $\{N_i\}^k$.
- The inference part is a collection of cells as $\{\{N_1\}^k, \{N_2\}^k, \dots\}$.

DPN has 40 convolutional layers altogether. The inference part is composed of 6 cells with increasing number of projection units: $(16^3, 16^3, 32^3, 32^3, 64^3, 64^3)$. The extraction and reconstruction part has 16 filters. Each projection unit has a depth 2. Due to the progressive design of pyramidal shape our DPN is much deeper (40 layers vs. 20 layers) but has no more parameters than VDSR.

C. Finetuning with internal priors

Internal priors are a powerful source of information but barely applied for deep learning architectures mainly due to the lack of internal examples and expensive training. We propose the adaptation to the internal priors of an input LR image as a finetuning to internal examples of the externally trained deep model. This strategy is applicable to other deep models such as VDSR.

Internal examples extraction The natural images exhibit a local recurrence of structures and textures within same and across different (coarser) image scales. This motivates our internal examples extraction. Each test LR image is down-scaled to form a pyramid of scaled images from which internal example LR-HR pairs are extracted.

Finetuning Our DPN model trained with external examples is first finetuned to the internally extracted examples such that to adapt to the internal priors of each test LR image. The super-resolved HR output is obtained using the finetuned DPN model. Different LR input images will have different adapted

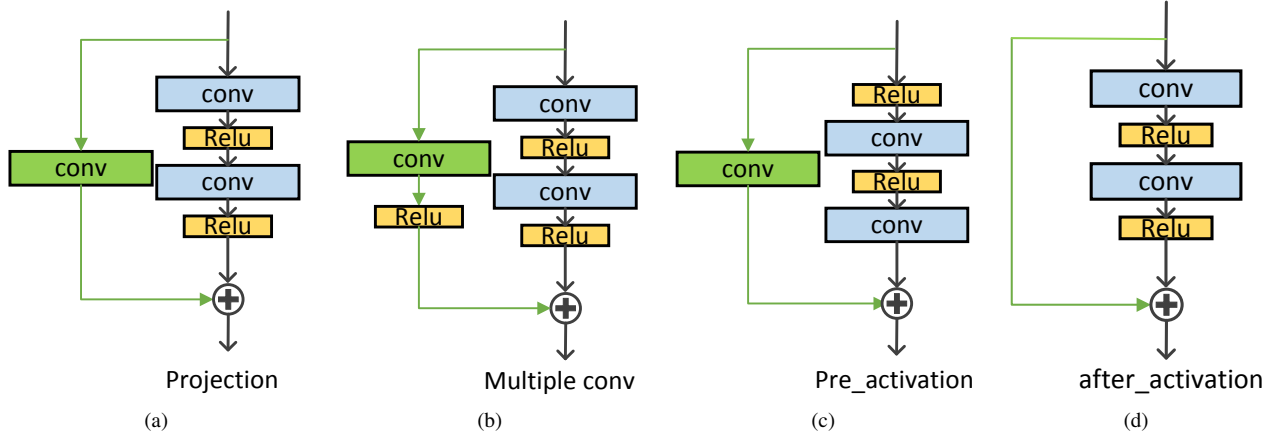


Fig. 3. Different architecture cells of CNN

models. It is a time expensive but performance superior approach. In our experiments, if *sufficient internal examples* or *strong self-similarities* exist, the model will be largely improved even within one training epoch.

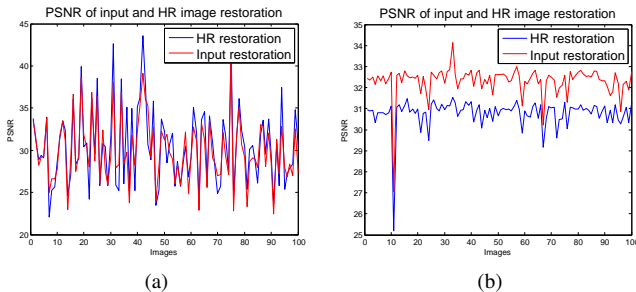


Fig. 4. PSNR (dB) curves of the input image restoration and HR image super-resolution on Urban100. The left corresponding to 100 randomly selected results from the 10000 restoration pairs, while the right corresponding to 100 restorations of 1 image (randomly selected).

D. Adaptation as a model selection

When facing with a test image, one can predict the HR image super-resolution performance of a model by evaluating the performance of input image restoration by this model. For Urban100 dataset, 100 models are finetuned for 100 LR images, respectively. For each LR image and the further downsampled image of it, we apply all these models to obtain the HR image and the restored LR input, respectively. In Fig. 4 we randomly selected 100 image and model pairs and show the achieved restoration performance in terms of Peak Signal to Noise Ratio (PSNR) dB. We note that the performances in each of the 100 pairs are highly correlated between starting from the LR input and starting from a further downsampled LR input, the ‘HR restoration’ and ‘Input restoration’ labels in Fig. 4. Thus, one can often predict the performance of a model on an image by checking the performance of the model on the downsampled image. Our adaptation as a model selection strategy is as follows:

- Offline train and store finetuned DPN (or other) models for hundreds of (diverse) images.

- Online apply the stored DPN (or other) models to a downsampled image of the input and check which of the models perform the best.
- Super-resolve the input LR image with the best selected model(s).

This adaptation as a model selection strategy is particularly useful when the test image is small (thus few internal examples) or when the finetuning/training is too expensive / infeasible. Often running a (deep) model is orders of magnitude faster than adapting it by finetuning with internal examples.

III. EXPERIMENTS

In this section, we conduct a series of experiments to compare the performance of our proposed DPN method against the state-of-the-art single image SR methods, especially to demonstrate the power of internal example adaptation. All the experiments use the deep learning toolbox `matconvnet` [23] and a single NVIDIA K40/K80 GPU card.¹

A. Experimental settings

Train dataset. We use 291 train images as in [14], [24], which include 91 images from Yang *et al.* [5] with the addition of 200 images from Berkeley Segmentation Dataset (BSD) [25].

Test datasets Five datasets are investigated: Set5 and Set14 from [6], Urban100 from [26] and BSD100 from [18], [27] and L20 from [13]. Specifically, Urban100 is famous for its self-similarities, L20 has very large images, between 3m pixels to up to 29m pixels, while the other datasets have images below 0.5m pixels.

As in [6], [15], [14], [24] we only super-resolve the luminance channel in YCrCb colorspace in our experiments and use the same downsizing operator (`imresize` from Matlab with `'bicubic'` interpolation) for obtaining the LR images from the ground truth HR images. All the training samples are randomly rotated or flipped as in [13], [14] with a size of 41×41 . DPN training uses batches of size 64, momentum and weight decay are set to 0.9 and 0.0001, respectively. We

¹We will publicly release both code and models upon paper acceptance.

train a single model for multiple scales with the same strategy as VDSR, which is mixing samples from all scales ($\times 2$, $\times 3$, and $\times 4$) randomly. The gradient clipping is applied as in [14]. Learning rate is initially set to 0.1 and then decreases by a factor of 10 every 30 epochs in logarithm manner which allow a smooth decreasing.

For internal finetuning, larger magnification factors can be achieved by upscaling small factors multiple times in a cascaded fashion [13], [28]. For internal example adaptations we report mainly for $\times 2$ magnification factor. Finetuning learning rate is fixed as $1e-4$ during model adaptation.

B. DPN with external examples

The performance of our DPN trained on external examples is quantitatively evaluated in terms of PSNR (dB) and SSIM measures on 4 datasets and for 3 upscaling factors. In Table I we report the results of our DPN in comparison with A+ [18] (a state-of-the-art neighbor embedding method), RFL [24] (a random forest approach using local regressors as in A+), SelfEx [26] (a self-exemplars method using internal priors), SRCNN [11] (revisited deep learning method), and VDSR [14], the very deep and current state-of-the-art CNN method. For all the compared methods we used the reported results or results achieved by original codes and models as provided by the authors. Bicubic interpolation results are provided for reference. In most of the settings our DPN achieves the best performance, especially for the $\times 3$ and $\times 4$ upscaling factors, while in the other cases, DPN is slightly (0.01dB) below VDSR.

Note that with our VDSR reimplementation and retraining we were not able to achieve the reported VDSR performance (more than 0.1dB gap in Set14). We hope that with the missing details of VDSR our model can be further improved.

C. Importance of preserving negative information

We conduct an ablation experiment for DPN on Set14. Table II shows the performance obtained with our reconstruction part which discards the ReLU layers. With a ReLU layer, the network failed to decrease the training loss or did not converge. First, all the convolutional skip connections have been changed into stacked plain layers which is a similar fashion like inception unit in Fig. 3(b). It broaden the width of the net. However, without the help of batch normalization, this structure failed to get good convergence with such a depth as our DPN net (40 layers) and got stuck with a high training loss and thus poor performance.

Then performance compared with convolutional skip vs. identity skip connections, and the positions of ReLU layers (ReLU before/after conv) as Fig. 3(c,d) respectively are represented in Table II for Set14. If ReLU comes after convolutional layers, the negative information will be discarded. Convolutional layers of the same depth among these networks have the same parameters. Note that in these experiments, a slightly different filter numbers of the extraction and reconstruction part has been applied so the performance is slightly different from Table I.

From the results in Table II, we conclude that preserving negative information is effective in two ways: either by our conv projection or by rearranging the order of convolutional and ReLU layers. Interestingly, conv projection which provides a stronger representational ability combined with a non-negative description achieves best performance. The combination of the two ways of preserving negative information has not brought more benefits.

D. Adaptation using internal contents

As the number of internal examples is limited especially when the input image is small, small stride and scale augmentation are applied. To demonstrate that our data specific finetuning approach is a generic way to improve deep model, we finetune not only our DPN but also VDSR and compare the average PSNR (dB) results on 5 datasets for $\times 2$ in Table III.

Not surprisingly, both DPN and VDSR largely improve after our adaptation, especially on Urban100 and L20 dataset (+0.23dB on Urban100 up to +0.3dB improvements on L20). The adapted DPN is 0.06dB better than the adapted VDSR on Urban100 and 0.05dB on L20. The visual comparisons with the state of art methods in Fig. 8 demonstrate that the adaptation keeps more details and sharper edges. Urban100 has strong self similarities while L20 has large size images and therefore provide a large number of internal examples for model finetuning. The poor improvement on BSD100 is mainly due to the fact that already we used 200 BSD images at training which have a similar peculiarity with BSD100.

1) *Performance vs. image size*: To analyze performance vs. image size, we need first to alleviate the influence of the self-similarities/contents. For this each ground truth (GT) HR image is bicubically downsized to produce GT images of lower sizes. The obtained GT images of different sizes share self-similarities/contents among themselves and with the originating HR image. Then by downsizing we generate LR input images and record the improvements achieved on these images by our adapted by finetuning methods. Let's take two large images from L20 for an example, one with high self-similarities and another with fewer recurrent structures. The original sizes are 4000×3000 and 5184×3456 . The images are downsized with a factor 1.25 per each to generated 11 GT images labeled from 1 to 11 from the largest size to the lowest. The performance improvements over the generic DPN are plotted in Fig. 5. The inflections of the curve are mainly due to the parameters changing as the image sizes become smaller than a threshold, we change the parameters (e.g. image pyramid scaling factor, strides) to extract more internal examples. We tried to keep a comparable number of extracted internal examples for each image, more than 10,000 for most of the images (including augmentation).

As expected the trend is to obtain smaller improvements with the smaller sizes of the input images which means that DPN is not able to pick sufficient internal priors for significant improvements. The same trend can be seen for the internal finetuning *w.r.t.* the magnification factor, as shown in Table IV. The larger the magnification factor / scale is the smaller the number of internal priors that can be used and, therefore, the smaller the gains are.

TABLE I
METHODS COMPARISON ON 4 DATASETS FOR 3 UPSCALING FACTORS IN TERMS OF AVERAGE PSNR AND SSIM MEASURES.

Dataset	Scale	Bicubic PSNR/SSIM	A+[18] PSNR/SSIM	RFL[24] PSNR/SSIM	SelfEx[26] PSNR/SSIM	SRCNN[11] PSNR/SSIM	VDSR[14] PSNR/SSIM	DPN (ours) PSNR/SSIM
Set5	$\times 2$	33.66/0.9299	36.54/0.9544	36.54/0.9537	36.49/0.9537	36.66/0.9542	37.53/0.9587	37.52 /0.9586
	$\times 3$	30.39/0.8682	32.58/0.9088	32.43/0.9057	32.58/0.9093	32.75/0.9090	33.66/0.9213	33.71/0.9222
	$\times 4$	28.42/0.8104	30.28/0.8603	30.14/0.8548	30.31/0.8619	30.48/0.8628	31.35/0.8838	31.42 /0.8849
Set14	$\times 2$	30.24/0.8688	32.28/0.9056	32.26/0.9040	32.22/0.9034	32.42/0.9063	33.03/0.9124	33.08 / 0.9129
	$\times 3$	27.55/0.7742	29.13/0.8188	29.05/0.8164	29.16/0.8196	29.28/0.8209	29.77/0.8314	29.80/ 0.8320
	$\times 4$	26.00/0.7027	27.32/0.7491	27.24/0.7451	27.40/0.7518	27.49/0.7503	28.01/0.7674	28.07/ 0.7688
BSD100	$\times 2$	29.56/0.8431	31.21/0.8863	31.16/0.8840	31.18/0.8855	31.36/0.8879	31.90/0.8960	31.89 /0.8958
	$\times 3$	27.21/0.7385	28.29/0.7835	28.22/0.7806	28.29/0.7840	28.41/0.7863	28.82/0.7976	28.84/0.7981
	$\times 4$	25.96/0.6675	26.82/0.7087	26.75/0.7054	26.84/0.7106	26.90/0.7101	27.29/0.7251	27.30/ 0.7256
Urban100	$\times 2$	26.88/0.8403	29.20/0.8938	29.11/0.8904	29.54/0.8967	29.50/0.8946	30.76/0.9140	30.82/ 0.9144
	$\times 3$	24.46/0.7349	26.03/0.7973	25.86/0.7900	26.44/0.8088	26.24/0.7989	27.14/0.8279	27.17/0.8282
	$\times 4$	23.14/0.6577	24.32/0.7183	24.19/0.7096	24.79/0.7374	24.52/0.7221	25.18/0.7524	25.25/ 0.7546

TABLE II
ABLATION COMPARISONS OF CONVOLUTIONAL SKIP VS IDENTITY SKIP CONNECTIONS, THE ORDER OF CONVOLUTION AND RELU LAYERS IN TERMS OF AVERAGE PSNR (dB) ON SET14.

scale	conv+ after_act	conv+ pre_act	identity+ after_act	identity+ pre_act
$\times 2$	33.05	32.95	32.97	33.01
$\times 3$	29.78	29.74	29.75	29.77
$\times 4$	28.08	28.03	28.02	28.02

TABLE III
AVERAGE PSNR (dB) COMPARISONS ON 5 DATASETS FOR $\times 2$ OF OUR DPN AND THE VDSR METHOD WITH AND WITHOUT ADAPTATION BY FINETUNING TO THE INTERNAL CONTENTS.

Method	Set5	Set14	BSD100	Urban100	L20
VDSR [14]	37.53	33.03	31.90	30.76	40.44
VDSR adapted	37.59	33.16	31.91	30.99	40.69
VDSR improvement	+0.07	+0.13	+0.01	+0.23	+0.25
DPN (ours)	37.52	33.08	31.89	30.82	40.44
DPN adapted	37.58	33.16	31.91	31.05	40.74
DPN improvement	+0.06	+0.08	+0.02	+0.23	+0.30

TABLE IV
PERFORMANCE OF ADAPTATION BY INTERNAL FINETUNING ON L20.

Scale	DPN adapted PSNR/SSIM	DPN PSNR/SSIM	gain
$\times 2$	40.74/0.9655	40.44/0.9650	+0.3db
$\times 3$	36.35/0.9226	36.17/0.9221	+0.18db
$\times 4$	33.85/0.8809	33.79/0.8808	+0.06db

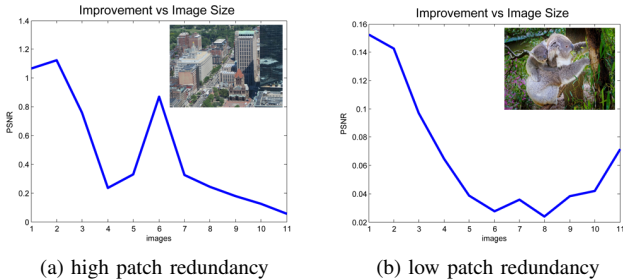


Fig. 5. PSNR (dB) improvement after DPN finetuning on each input image of different sizes. The images are ordered from the largest '1' to the smallest '11' size.

2) *Performance vs. finetuning epochs*: In Fig. 6 we plot the average performances over L20 and Urban100 datasets

achieved by both DPN and VDSR when adapted by finetuning on internal examples from the LR test image. We vary the number of epochs used in the finetuning and report the average performance over the whole datasets. One single epoch (all the internal examples were backpropagated once) for adaptation makes a large difference, as most of the improvement over the baseline generic methods is achieved after a single finetuning epoch. After a couple of epochs, the improvement peaks and reaches a plateau.

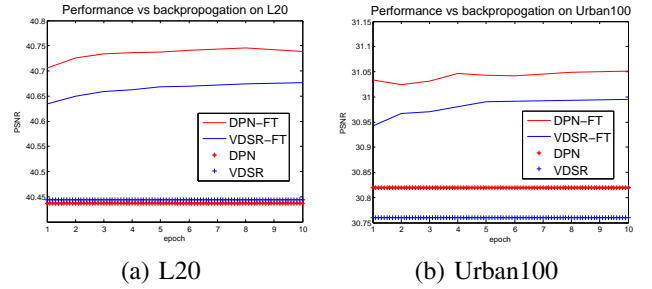


Fig. 6. Average PSNR (dB) performance of VDSR and our DPN method vs. finetuning epochs on L20 and Urban100 datasets in comparison with the generic externally trained VDSR and DPN methods.

3) *Runtime analysis*: Internal adaptation is a time expensive but performance superior approach. The runtime efficiency is closely related to the number of internal examples considered. When limited number of internal examples are used from the LR image (such as by loosely sampling them with a large stride or without scale augmentation which applies the input image to form a image pyramid), the adaptation in one epoch can be fast, as the input LR image is smaller. In fact, the number of internal examples depends on the parameters applied. The performance, running time and parameters are reported in Table V. Note that only the stride parameter is different for Urban100 between columns and only with and without scale augmentation is different for L20.

The number of internal examples and the stride are related by $(\text{floor}((\text{imgSz}_1 - \text{subimgSz})/\text{stride}) + 1) \times (\text{floor}((\text{imgSz}_2 - \text{subimgSz})/\text{stride}) + 1)$. imgSz and subimgSz are the size of the images and examples respectively. The size For typical Urban100 images with size 1024×1024 (input LR images 512×512) there are 576 samples for a stride of 20.

TABLE V
INTERNAL FINETUNING PERFORMANCE AND RUNTIME VS. PARAMETER SETTINGS

Urban100 (PSNR/gain/time)	DPN 30.82/-/-	stride20 30.87/+0.05/7.2s	stride5 31.04/+0.22/97.3s	performance in plateau 31.05/+0.23/389.2s
L20 (PSNR/gain/time)	DPN 40.44/-/-	single scale 40.61/+0.17/100.5s	scale augmentation 40.71/+0.27/288.7s	performance in plateau 40.74/0.30/1154.8s

According to Table V and Fig. 6, one single epoch (all internal examples are backpropagated once) of adaptation accounts for the greatest gain over the baseline and the performance converges after a couple of epochs. Extracting internal examples for Urban100 with a stride 20 and finetune the model in one epoch (7.2 seconds) improves the performance by 0.05dB, and after 5 epochs (36.0s) by 0.13dB.

In addition, data augmentation further improves at computation cost. Since even without augmentation the performance improvement is clear, the operation can be activated whenever the application needs it. For medium size images DPN adaptation takes ~ 1 minute but the parameters can tradeoff speed for performance.

E. Adaptation using internal contents and external augmentation

Adaptation using internal contents and external augmentation means finetuning the model to the internal examples of the LR image plus other external examples which are similar to the internal ones. This proves to be effective when we find similar examples.

- Internal examples are extracted.
- External examples which has strong similarities are prepared for corresponding internal examples.
- Mixing internal examples and corresponding external examples together.
- Finetuning the model using these mixtures of internal contents and external augmentation.

In the following we give an example of how external augmentation can help when we find (very) similar examples. The ground truth images of Set14 were downsampled by a factor of 1.25 and used as external images. Then with a mixing of external and internal examples, the performance boosted as shown in Table VI denoted by ‘adapted DPN+aug(images)’. This experiment demonstrated that with an proper (ideal) external example augmentation, the adaptation using internal contents and external augmentation can work. With a fast image retrieval technique this strategy could be very effective even for very small images. Moreover, if a large and diverse external example set is prepared and each internal example could find some external examples which have strong similarities by by some efficient and effective nearest search methods or matching methods like PatchMatch [29]. Larger improvements are expected and this strategy will be explored in the future.

F. Adaptation as a model selection

In the next we described a couple of experiments involving the selection of models from a pool of trained models.

TABLE VI
DPN PERFORMANCE COMPARISON WITH AND WITHOUT ADAPTATION TO INTERNAL CONTENTS AND EXTERNAL AUGMENTATION ON SET14 WITH MAGNIFICATION $\times 2$.

	DPN	adapted DPN	adapted DPN+aug(images)
PSNR (dB)	33.08	33.16	33.29

1) *Experiment 1:* We used the adaptation using internal contents as described in Section II-D to finetune 20 DPN models corresponding to the L20 images in addition to the original DPN model and test them on Set14 images with $\times 2$. By choosing the best 3 models out of 20 for restoration, as reflected by the performance on the downsampled LR images, the results slightly improve to 33.12dB *w.r.t.* the generic VDSR with 33.03dB. Although it is a marginal improvement, partly due to the large mismatch between the L20 and Set14 images, this strategy has a great potential. Various strategies can be devised to train a set of SR models specialized on (semantically) different images and image contexts (such as cartoons, flowers, skyscrapers, villages, dogs).

TABLE VII
A SUCCESSFUL MODEL SELECTION EXAMPLE

		model			
image tested on	image adapted to	VDSR		DPN	
		img47	img72	img47	img72
img47		26.52	26.29	26.69	26.22
img72		25.52	26.13	25.60	26.40

2) *Experiment 2:* In a second experiment, we take two images from Urban100, image 47 and image 72. In contrast to the previous experiment the two images share similar contents and, in this case, their finetuned VDSR / DPN models work very well for each other. As shown Table VII, testing image 47, with the VDSR model finetuned on image 72 brings an improvement of 0.41dB over the generic VDSR, while on the counterpart, testing image 72, with the VDSR model finetuned on image 47 shows an improvement of 0.30dB. On the same images our DPN works better than VDSR improving 0.05dB on image 47 and 0.26dB on image 72 and when using the finetuned DPN models we see the same behavior as for VDSR. The images 47 and 72 and the SR results of our DPN method are found in Fig 7. These experimental results show the potential of model selection if the pool of models are large and diverse enough.

3) *Experiment 3:* The performance of a model for the ‘input restoration’ and ‘HR image super-resolution’ is highly correlated as shown in Section II-D.

In Table VIII for Urban100 dataset and $\times 2$ we compare our DPN with DPN with internal adaptation (DPN(A)), and

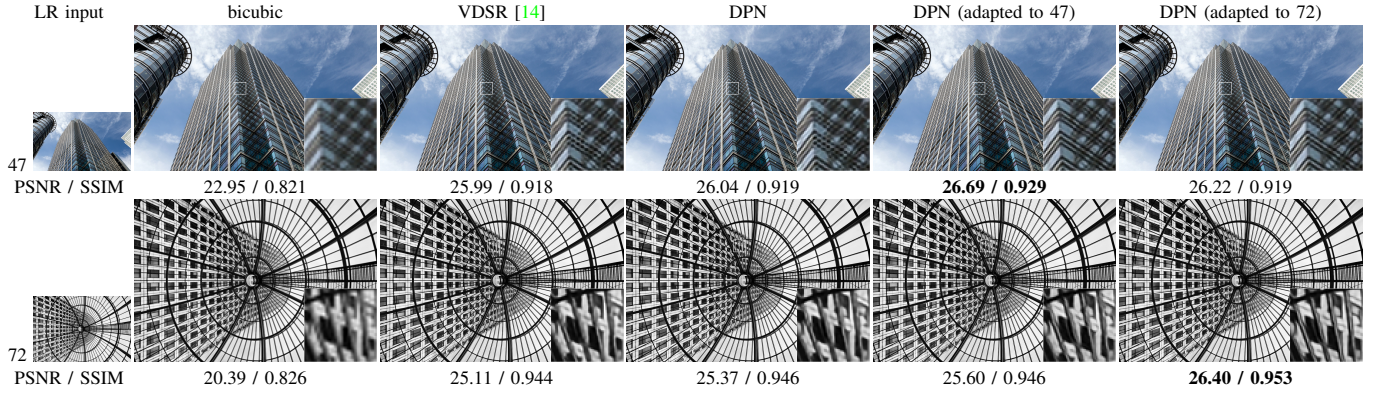


Fig. 7. SR $\times 2$ results on Urban100 images 47 and 72 whose finetuned models (on each LR image) work well for each other.



Fig. 8. SR results for our methods – DPN and DPN adapted by internal finetuning methods – in comparison with VDSR [14], SRCNN [11], bicubic interpolation and ground truth image. The cropped patches are of size 25×25 pixels. The bottom 3 images are from L20 while the first is from Set14.

given 100 DPN models built on the low resolution Urban images, our selection strategy based on the LR input image and its downscaled version (Selection), the oracle selection of the best model (Selection(O)), and our selection strategy from a random subset of 10 models (Random Selection(10)). Our selection strategy picks the best model according to the performance of restoring LR input image from downscaled LR images. The Table VIII demonstrates that our model selection strategy is effective as an alternative way for model adaptation by finetuning, both achieving +0.23dB improvements. For 80 Urban images the model selection strategy led to better

performance than the DPN generic model. Noteworthy is that that a random selection strategy harms the performance while the optimal /oracle selection strategy leads to only 0.14dB better performance than the proposed strategy.

TABLE VIII
MODEL SELECTION VS INTERNAL ADAPTATION ON URBAN100 AND $\times 2$

Method	DPN	DPN (A)	Selection (ours)	Selection (O)	Random Selection(10)
PSNR gain	30.82	31.05	31.05	31.19	30.29
	–	+0.23	+0.23	+0.37	-0.53

IV. MODEL ADAPTATION WITH INTERNAL EXAMPLES VS. BACK-PROJECTION AND ENHANCEMENT

Our model adaptation with internal examples mainly depends on the self-similarities of the images. We compare the (A)adaptation to the LR image by use of internal examples with two other techniques known to further improve the performance of a SR method: (B)back-projection [30] and (E)enhanced prediction [13]. As in [13], iterative back projection (B) refinement makes the HR reconstruction consistent with the LR input. (E) enhancement means to enhanced the restoration by averaging the predictions on a set of transformed images derived from it. For SR image, after rotations and flips, the same HR results at pixel level should be generated. Therefore, a set of 8 LR images were generated as we apply rotations and flips on the LR image as [13], then apply the SR method on each, reverse the transformation on the HR outputs and average for the final HR result.

From the Table IX, some conclusions can be obtained:

- Model adaptation (A) with internal examples, back-projections(B) and enhancement(E) are all effective way to improve performance.
- For images with redundant contents/ high self-similarities as in L20 or Urban100, model adaptation (A) with internal examples which is especially common in larger and larger nowadays images, is more effective than the other techniques.
- The combination of techniques bring larger gains which indicates complementarity. DPN+(A+E) gain +0.4dB over DPN on both Urban100 and L20 while DPN+(E) gets only +0.1dB.

Thus we hope to arouse the interests of the communities for the internal example priors adaptation which can be combined with other techniques to further improve the situations.

V. DISCUSSION

The large improvements achieved by model adaptation to the input image demonstrates the power of internal example priors. Also, it is an indicator that the representation ability of a deep CNN with certain parameters is far from its limit. Our DPN starts from architecture design and external example prior modeling. It benefits from reducing the training difficulties and increasing the representational ability with a projection skip connection as well as information preserving reconstruction design. Moreover, when redundant contents / high self-similarities exist, which is especially common in larger and larger nowadays images, the super-resolution results can be largely improved by simple finetuning adaption of the deep model to internal examples to the input image. A model selection strategy is proposed which is proved to be efficient and effective if the pool of models are large and diverse enough. In addition, when internal prior is combined with (B) back-projection and/or (E) enhanced prediction, it leads to extra performance gains which indicates the complementarity of these techniques. To the best of our knowledge our work is the first to study adaptation of deep models for single-image super-resolution. We want to arouse the interests of communities to focus on the internal priors which are limited

but has been proved effective, and highly relevant. In the future, deep architectures to directly model internal priors will be explored.

VI. CONCLUSION

We proposed a novel deep architecture for single image super-resolution and studied a couple of ways to adapt the externally learned deep models to the content of the low-resolution image input. With our proposed method we are able to improve over the state-of-the-art deep learning method (VDSR) on standard benchmarks. The adaptation to the content proved successful in most of the cases, significant improvements being achieved especially for medium to large images with redundant contents / high self-similarities.

ACKNOWLEDGMENT

This work is partially supported by National Science Foundation of China under Grant NO. 61473219, and the National Basic Research Program of China (973 Program) under Grant No. 2015CB351705.

REFERENCES

- [1] R. Keys, "Cubic convolution interpolation for digital image processing," *Acoustics, Speech and Signal Processing, IEEE Transactions on*, vol. 29, no. 6, pp. 1153–1160, 1981. 1
- [2] M. Irani and S. Peleg, "Motion analysis for image enhancement: Resolution, occlusion, and transparency," *Journal of Visual Communication and Image Representation*, vol. 4, no. 4, pp. 324–335, 1993. 1
- [3] H. A. Aly and E. Dubois, "Image up-sampling using total-variation regularization with a new observation model," *Image Processing, IEEE Transactions on*, vol. 14, no. 10, pp. 1647–1659, 2005. 1
- [4] W. T. Freeman, E. C. Pasztor, and O. T. Carmichael, "Learning low-level vision," *International journal of computer vision*, vol. 40, no. 1, pp. 25–47, 2000. 1
- [5] J. Yang, J. Wright, T. Huang, and Y. Ma, "Image super-resolution as sparse representation of raw image patches," in *Computer Vision and Pattern Recognition, 2008. CVPR 2008. IEEE Conference on*. IEEE, 2008, pp. 1–8. 1, 2, 4
- [6] R. Timofte, V. De, and L. V. Gool, "Anchored neighborhood regression for fast example-based super-resolution," in *Computer Vision (ICCV), 2013 IEEE International Conference on*. IEEE, 2013, pp. 1920–1927. 1, 2, 4
- [7] D. Glasner, S. Bagon, and M. Irani, "Super-resolution from a single image," in *Computer Vision, 2009 IEEE 12th International Conference on*. IEEE, 2009, pp. 349–356. 1
- [8] G. Freedman and R. Fattal, "Image and video upscaling from local self-examples," *ACM Transactions on Graphics (TOG)*, vol. 30, no. 2, p. 12, 2011. 1
- [9] M. Zontak and M. Irani, "Internal statistics of a single natural image," in *Computer Vision and Pattern Recognition (CVPR), 2011 IEEE Conference on*. IEEE, 2011, pp. 977–984. 1
- [10] H. Chang, D.-Y. Yeung, and Y. Xiong, "Super-resolution through neighbor embedding," in *Computer Vision and Pattern Recognition, 2004. CVPR 2004. Proceedings of the 2004 IEEE Computer Society Conference on*, vol. 1. IEEE, 2004, pp. 1–275. 1, 2
- [11] C. Dong, C. C. Loy, K. He, and X. Tang, "Image super-resolution using deep convolutional networks," *IEEE transactions on pattern analysis and machine intelligence*, vol. 38, no. 2, pp. 295–307, 2016. 1, 2, 5, 6, 8
- [12] J. Yang, Z. Lin, and S. Cohen, "Fast image super-resolution based on in-place example regression," in *Computer Vision and Pattern Recognition (CVPR), 2013 IEEE Conference on*. IEEE, 2013, pp. 1059–1066. 1
- [13] R. Timofte, R. Rothe, and L. Van Gool, "Seven ways to improve example-based single image super resolution," in *Proceedings of the IEEE Conference on Computer Vision and Pattern Recognition*, 2016, pp. 1865–1873. 1, 4, 5, 9

TABLE IX
PERFORMANCE COMPARISONS BETWEEN MODEL ADAPTATION WITH INTERNAL EXAMPLES (A), BACK-PROJECTION (B) AND ENHANCED PREDICTION (E) FOR MAGNIFICATION $\times 2$. PSNR AND GAIN ARE MEASURED IN DB.

	DPN PSNR/SSIM	DPN+(A) PSNR/SSIM	DPN+(B) PSNR/SSIM	DPN+(E) PSNR/SSIM	DPN+(A+B) PSNR/SSIM	DPN+(A+E) PSNR/SSIM
Set5	37.52 / 0.9586	37.58 / 0.9588	37.56 / 0.9589	37.64 / 0.9592	37.64 / 0.9591	37.70 / 0.9594
gain vs. DPN	–	0.06	0.04	0.12	0.12	0.18
Set14	33.08 / 0.9129	33.16 / 0.9132	33.11 / 0.9133	33.18 / 0.9138	33.20 / 0.9136	33.27 / 0.9143
gain vs. DPN	–	0.08	0.03	0.10	0.12	0.19
BSD100	31.89 / 0.8958	31.91 / 0.896	31.91 / 0.8961	31.96 / 0.8967	31.93 / 0.8963	31.97 / 0.8967
gain vs. DPN	–	0.02	0.02	0.07	0.04	0.08
Urban100	30.82 / 0.9144	31.05 / 0.9161	30.85 / 0.9148	30.95 / 0.9159	31.11 / 0.9167	31.21 / 0.9179
gain vs. DPN	–	0.23	0.03	0.13	0.29	0.39
L20	40.44 / 0.965	40.74 / 0.9655	40.49 / 0.9653	40.56 / 0.9655	40.78 / 0.9657	40.84 / 0.9659
gain vs. DPN	–	0.30	0.05	0.12	0.34	0.40

- [14] J. Kim, J. K. Lee, and K. M. Lee, “Accurate image super-resolution using very deep convolutional networks,” in *Proceedings of the IEEE Conference on Computer Vision and Pattern Recognition*, 2016. [1](#), [2](#), [4](#), [5](#), [6](#), [8](#)
- [15] C. Dong, C. C. Loy, K. He, and X. Tang, “Learning a deep convolutional network for image super-resolution,” in *Computer Vision—ECCV 2014*. Springer, 2014, pp. 184–199. [1](#), [2](#), [4](#), [8](#)
- [16] H. C. Burger, C. Schuler, and S. Harmeling, “Learning how to combine internal and external denoising methods,” in *German Conference on Pattern Recognition*. Springer, 2013, pp. 121–130. [1](#)
- [17] W. Dong, L. Zhang, G. Shi, and X. Li, “Nonlocally centralized sparse representation for image restoration,” *IEEE Transactions on Image Processing*, vol. 22, no. 4, pp. 1620–1630, 2013. [1](#)
- [18] R. Timofte, V. De Smet, and L. Van Gool, “A+: Adjusted anchored neighborhood regression for fast super-resolution,” in *Computer Vision—ACCV 2014*. Springer, 2014, pp. 111–126. [2](#), [4](#), [5](#), [6](#)
- [19] K. He, X. Zhang, S. Ren, and J. Sun, “Deep residual learning for image recognition,” in *Proceedings of the IEEE Conference on Computer Vision and Pattern Recognition*, 2016, pp. 770–778. [2](#)
- [20] K. Simonyan and A. Zisserman, “Very deep convolutional networks for large-scale image recognition,” *arXiv preprint arXiv:1409.1556*, 2014. [2](#)
- [21] K. He, X. Zhang, S. Ren, and J. Sun, “Identity mappings in deep residual networks,” in *European Conference on Computer Vision*. Springer, 2016, pp. 630–645. [2](#)
- [22] C. Dong, C. C. Loy, and X. Tang, “Accelerating the super-resolution convolutional neural network,” in *European Conference on Computer Vision*. Springer, 2016, pp. 391–407. [2](#), [3](#)
- [23] A. Vedaldi and K. Lenc, “Matconvnet – convolutional neural networks for matlab,” *CoRR*, vol. abs/1412.4564, 2014. [4](#)
- [24] S. Schuler, C. Leistner, and H. Bischof, “Fast and accurate image upscaling with super-resolution forests,” in *Proceedings of the IEEE Conference on Computer Vision and Pattern Recognition*, 2015, pp. 3791–3799. [4](#), [5](#), [6](#)
- [25] D. Martin, C. Fowlkes, D. Tal, and J. Malik, “A database of human segmented natural images and its application to evaluating segmentation algorithms and measuring ecological statistics,” in *Computer Vision, 2001. ICCV 2001. Proceedings. Eighth IEEE International Conference on*, vol. 2. IEEE, 2001, pp. 416–423. [4](#)
- [26] J.-B. Huang, A. Singh, and N. Ahuja, “Single image super-resolution from transformed self-exemplars,” in *2015 IEEE Conference on Computer Vision and Pattern Recognition (CVPR)*. IEEE, 2015, pp. 5197–5206. [4](#), [5](#), [6](#)
- [27] C.-Y. Yang, C. Ma, and M.-H. Yang, “Single-image super-resolution: A benchmark,” in *Computer Vision—ECCV 2014*. Springer, 2014, pp. 372–386. [4](#)
- [28] Z. Wang, D. Liu, J. Yang, W. Han, and T. Huang, “Deep networks for image super-resolution with sparse prior,” in *Proceedings of the IEEE International Conference on Computer Vision*, 2015, pp. 370–378. [5](#)
- [29] C. Barnes, E. Shechtman, A. Finkelstein, and D. Goldman, “Patchmatch: a randomized correspondence algorithm for structural image editing,” *ACM Transactions on Graphics-TOG*, vol. 28, no. 3, p. 24, 2009. [7](#)
- [30] M. Irani and S. Peleg, “Improving resolution by image registration,” *CVGIP: Graphical models and image processing*, vol. 53, no. 3, pp. 231–239, 1991. [9](#)